View metadata, citation and similar papers at core.ac.uk

brought to you by CORE

provided by Boise State University - ScholarWorks

Boise State University
ScholarWorks

Geosciences Faculty Publications and Presentations | Department of Geosciences

7-1-2018

Hyporheic Source and Sink of Nitrous Oxide

W. Jeffery Reeder
University of Idaho

Annika M. Quick
Boise State University

Tiffany B. Farrell
Boise State University

Shawn G. Benner
Boise State University

Kevin P. Feris
Boise State University

See next page for additional authors

This document was originally published in *Water Resources Research* by Wiley on behalf of the American Geophysical Union. Copyright restrictions may apply. doi:10.1029/2018WR022564

Authors
W. Jeffery Reeder, Annika M. Quick, Tiffany B. Farrell, Shawn G. Benner, Kevin P. Feris, Alessandra Marzadri, and Daniele Tonina

This article is available at ScholarWorks: https://scholarworks.boisestate.edu/geo_facpubs/434

Water Resources Research

RESEARCH ARTICLE
10.1029/2018WR022564

Hyporheic Source and Sink of Nitrous Oxide

W. Jeffery Reeder[1], Annika M. Quick[2,3], Tiffany B. Farrell[4], Shawn G. Benner[2], Kevin P. Feris[4], Alessandra Marzadri[1], and Daniele Tonina[1]

[1]Department of Civil Engineering, University of Idaho, Moscow, ID, USA, [2]Department of Geosciences, Boise State University, Boise, ID, USA, [3]Earth and Planetary Science Department, Harvard University, Cambridge, MA, USA, [4]Department of Biologic Sciences, Boise State University, Boise, ID, USA

Key Points:
- Only a portion of the flowlines through the hyporheic are likely to emit N_2O, while others will sink N_2O to below instream concentrations
- A framework for identifying the source location of N_2O emissions at the flowline level is presented
- Peak N_2O production occurs in portions of a bedform with relatively high hyporheic velocities and intermediate residence times

Correspondence to:
W. J. Reeder,
wjreeder@uidaho.edu

Citation:
Reeder, W. J., Quick, A. M., Farrell, T. B., Benner, S. G., Feris, K. P., Marzadri, A., & Tonina, D. (2018). Hyporheic source and sink of nitrous oxide. *Water Resources Research*, *54*, 5001–5016. https://doi.org/10.1029/2018WR022564

Received 9 JAN 2018
Accepted 29 JUN 2018
Accepted article online 7 JUL 2018
Published online 26 JUL 2018

Abstract Nitrous oxide (N_2O) is a potent greenhouse gas with an estimated 10% of anthropogenic N_2O coming from the hyporheic zone of streams and rivers. However, difficulty in making accurate fine-scale field measurements has prevented detailed understanding of the processes of N_2O production and emission at the bedform and flowline scales. Using large-scale, replicated flume experiments that employed high-density chemical concentration measurements, we have been able to refine the current conceptualization of N_2O production, consumption, and emission from the hyporheic zone. We present a predictive model based on a Damköhler-type transformation ($\tilde{\tau}$) in which the hyporheic residence times (τ) along the flowlines are multiplied by the dissolved oxygen consumption rate constants for those flowlines. This model can identify which bedforms have the potential to produce and emit N_2O, as well as the portion and location from which those emissions may occur. Our results indicate that flowlines with $\tilde{\tau}_{up}$ ($\tilde{\tau}$ as the flowline returns to the surface flow) values between 0.54 and 4.4 are likely to produce and emit N_2O. Flowlines with $\tilde{\tau}_{up}$ values of less than 0.54 will have the same N_2O as the surface water and those with values greater than 4.4 will likely sink N_2O (reference conditions: 17C, surface dissolved oxygen 8.5 mg/L). N_2O production peaks approximately at $\tilde{\tau} = 1.8$. A cumulative density function of $\tilde{\tau}_{up}$ values for all flowlines in a bedform (or multiple bedforms) can be used to estimate the portion of flowlines, and in turn the portion of the streambed, with the potential to emit N_2O.

Plain Language Summary Nitrous oxide (N_2O) is a potent greenhouse gas that has been increasing its atmospheric warming impact. Globally, an estimated 10% of the N_2O that is released to the atmosphere comes from rivers and streams. These emissions are strongly correlated to nitrogen compounds from industrial and agricultural runoff. However, not all streams that are impacted emit N_2O. Clearly, streams have some control over the chemical activity that occurs within their banks. However, the large-scale studies that have provided the global estimates of N_2O emissions have not been able to pinpoint the mechanisms that control emissions or where within a steam emissions originate. Most of the chemical activity in rivers and streams occurs within the sediments directly adjacent to the stream flow. This volume of saturated sediments is called the hyporheic zone. Surface water flows into the hyporheic sediments carrying with it dissolved chemicals and eventually returns to the surface flow carrying reacted chemical products, potentially among these is N_2O. We demonstrate that this flow exerts control over the biological processes that are the primary source of N_2O emissions from rivers and streams and present a mathematical model that predicts which flowlines have the correct properties to produce and emit N_2O.

1. Introduction

Nitrous oxide (N_2O) is a potent greenhouse gas that is of particular interest because of its role in the depletion of stratospheric ozone. On an equal mass basis, N_2O has 300 times the forcing potential as CO_2 (IPCC, 2007). Due to actions taken in response to *The Montreal Protocol on Substances that Deplete the Ozone Layer* (MP), the abundance of anthropogenically generated, ozone-depleting substances that are controlled by the MP have been steadily decreasing over the past few decades. However, N_2O is not among the substances included in the MP and in the time since its implementation, N_2O concentrations in the upper atmosphere have been steadily increasing, raising the prominence of N_2O as a cause for ozone depletion and as a forcing agent for atmospheric warming (Ravishankara et al., 2009; World Meteorological Organization (WMO), 2014; Wuebbles, 2009). Recent estimates indicate that N_2O is responsible for 9% of the current climate forcing (Rosamond et al., 2012). Streams and rivers have been identified as a significant source of N_2O emissions. Estimates of N_2O emissions from streams and rivers vary in range from 0.1 Tg N-N_2O/year (Anderson et al.,

©2018. American Geophysical Union. All Rights Reserved.

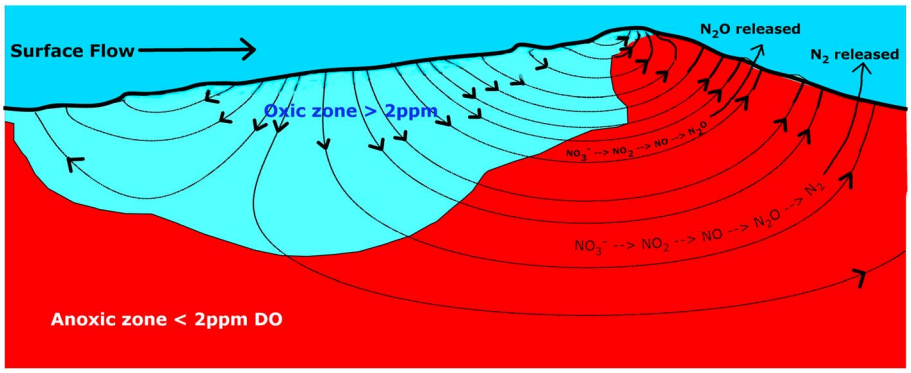

Figure 1. A conceptual model of reactive solute transport through the hyporheic zone. Because of pressure gradients along the bed surface, surface water flows into the bed sediments carrying with it DO and reactive nitrogen compounds. DO is consumed through aerobic respiration by microbes in the hyporheic zone. Some short flowlines return to the surface before all DO is consumed. For longer flowlines, DO is consumed to below 2 ppm and anaerobic respiration (in this case, denitrification) is initiated (Beaulieu et al., 2008; Chapelle, 1993; Tiedje, 1988). For long flowlines, N_2 gas is the primary effluent. The effluent from medium-length flowlines is likely to include intermediate reaction products. The emission of N_2O, an intermediate of denitrification, is of particular concern and is illustrated here. DO = dissolved oxygen; N_2O = nitrous oxide.

2010) to 0.95 Tg N-N_2O/year (Seitzinger & Kroeze, 1998). In the middle of this range, Beaulieu (2011) estimated emissions from streams at 0.68 Tg N-N_2O/year, which is approximately 10% of all anthropogenically generated N_2O that is emitted into the atmosphere. These emissions are largely correlated to pollutant runoff from wastewater treatment plants and agricultural practices (Davidson, 2009) with excess nitrogen stimulating N_2O production in rivers (McMahon & Dennehy, 1999; Park et al., 2012). However, field observations indicate that not all impacted streams emit N_2O (Beaulieu, 2011).

Our current understanding of these emissions comes almost exclusively from reach or watershed-scale field studies (Beaulieu, 2011; Beaulieu et al., 2008; Laursen & Seitzinger, 2004; Zarnetske et al., 2011a, 2011b) or from numerical studies (Marzadri, Tonina, Bellin, et al., 2014; Marzadri et al., 2011), conducted at similar scales. While these studies and models have been quite useful in quantifying the regional and global impact of N_2O emissions from streams, they have been unable to resolve the source points of emission at the hyporheic flowline scale or even bedform scale. Recently, Quick et al. (2016) presented a conceptual model in which only the portion of the hyporheic zone (HZ) that contains flowlines with intermediate residence times produce and emit N_2O. Portions of the HZ with short or long residence time have dissolved oxygen (DO; short flowlines) or N_2 (long flowlines) as their primary emissions. However, this work did not provide a method to delineate the emitting zone nor a procedure to identify and quantify short, intermediate, or long residence times. Having an understanding of N_2O emissions at the flowline scale becomes important when trying to define the mechanisms that lead to and control N_2O emissions from streams. This level of understanding could usefully supplement planning and assessment of remediation and restoration projects whose objectives include reducing N_2O emissions (Herzog et al., 2016). Our goal in this study is to resolve the controls on N_2O production and emission and to create a model (Figure 1) that resolves N_2O production at the flowline scale and can be scaled up to the bedform, reach, or watershed scale.

2. Methods and Materials

2.1. Experimental Setup

The experimental setup and methodologies were described in detail in Quick et al. (2016). The key elements are described below. We conducted two sets of experiments in the large-scale flume (approximately 20 × 2 m) at the Center for Ecohydraulics Research Stream Laboratory (Budwig & Goodwin, 2012) at the University of Idaho, Boise, to test the impact of bed morphology, stream hydraulics, and surface water chemistry (reactive nitrogen loading) on DO and nitrogen consumption dynamics and the impact of those processes on N_2O emissions from streams. The first experiment (Flume 1) ran continuously from August 2013 through December 2013, and the second (Flume 2) ran from February 2015 through June 2015. In both sets of experiments, the flume was divided into three stream channels (30 cm wide × 60 cm deep × 15 m long) which were

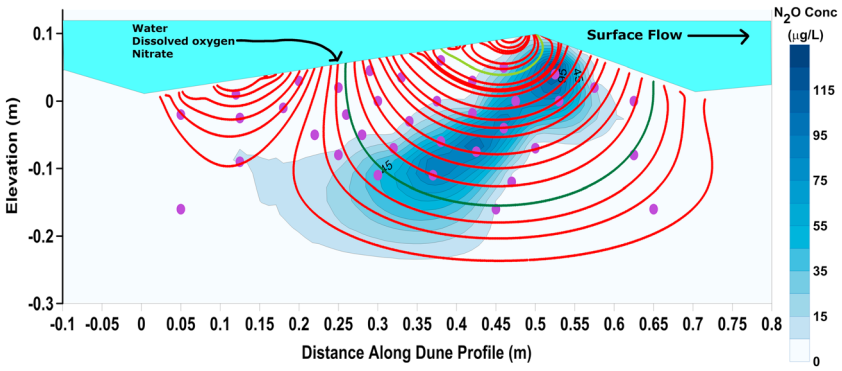

Figure 2. The measured and krigged N_2O concentration profiles and the calculated flowlines (red and green traces) for the Channel C, 70 cm dune on Day 91 of the Flume 2 experiment. The green traces mark the flowlines for the N_2O versus τ profiles in Figure 3. N_2O = nitrous oxide.

separated by access corridors. Triangular dunes of various sizes were constructed from 90% quarry sand (D_{50} ~1.5 mm) and 10% natural sand collected from the Boise River (Boise, ID, USA). The natural sand provided an inoculum to initiate bacterial communities, which were representative of those that typically reside in streambed sediments. To provide an organic carbon nutrient source, 0.15% by dry weight of finely divided (<5 mm) cottonwood leaves were uniformly added to the sand mix. Water for surface flow over the dunes was pumped and recirculated from a 190,000-L catch basin into a head box at the top of the flume and over individual sills into each of the three flume channels. We will consider three different dune variants. From Flume 1, we evaluate the response of a 9 cm tall by 1 m long dune (two replicates), hereafter referred to as the *9 cm dune*. The energy slope for the 9 cm dune was 0.002. The concentration of nitrate in the surface water (from KNO_3 added to the catch basin) was approximately 3 mg/L in Flume 1. From Flume 2, we consider a 9 cm tall by 100 cm long dune and a 9 cm tall by 70 cm long dune, hereafter referenced as *100 cm dune* and *70 cm dune*, respectively. The three replicate channels in Flume 2 are referred to as Channels A, B, and C. Individual dunes in Flume 2 are identified by their channel and length, that is, a 70 cm dune in Channel C is identified as *C70*. The energy slope for the Flume 2 experiments was 0.003. In Flume 2, the surface-water nitrate concentration was approximately 10 mg/L. In both experiments, we surveyed bed surface and water surface profiles every 2 cm along the centerline of each dune with a laser and an ultrasonic sensor, respectively; both with better than 1 mm vertical resolution.

2.2. Pore Water Sampling

In situ pore-water-extraction ports (rhizon soil-moisture samplers, Rhizosphere Research Products, Netherlands) were embedded through the sidewalls of the flume channels and into the bulk of the dunes, allowing us to obtain high-density, repeatable pore water samples throughout the duration of the experimental runs. A typical placement of the in situ sampling ports is illustrated by the purple dots in Figure 2. The embedded portion of the rhizon sampling ports consisted of porous (0.45 μm) tubing (10 cm × 3 mm) that was supported by a stainless steel wire stiffener. The porous tube was connected through the sidewall of the flume channel and into the access corridors by silicon tubing that was terminated by a luer lock adapter and a cap. During sampling, the cap was replaced with a needle and, initially, the port was allowed to drip for a brief time to allow any stagnant water in the silicon tubing to be evacuated. For the actual pore water sample, a closed sampling method was used. The needle was inserted, under water, through the septa of an evacuated vial. Pore water was slowly pulled by the vacuum in the vial through the rhizon sampling port and into the vial. The vial was held under water for the duration of the sample extraction. Approximately 10 ml of pore water was collected in a 20 ml headspace vial. To measure dissolved N_2O, the samples were analyzed using an HP 7694 headspace autosampler and an Agilent 6890 gas chromatograph equipped with a GS_Carbon PLOT column (30 m × 0.53 mm) and a ^{63}Ni microelectron capture detector. Dissolved concentrations of N_2O were calculated using Henry's law (Hudson, 2004).

2.3. Bed-Surface Pressure Profiles and Hyporheic Flowlines

The interaction between surface flow velocities and streambed morphology creates the bed surface pressure profile that drives hyporheic flow (Elliott & Brooks, 1997). That pressure profile also constitutes the boundary

conditions for the groundwater flow equations that describe hyporheic flows. Because of the low surface flow velocities used in the flume experiments (<0.1 m/s), the bed surface pressures were functionally unmeasurable. As a result, we modeled the pressure profiles (Cardenas & Wilson, 2007) using ANSYS Fluent CFD (ANSYS Inc., Canonsburg, PA, USA). Fluent provides a numerical solution to the Reynolds-Averaged, Navier Stokes equations. The Fluent models were meshed with between 65,000 and 95,000 triangular elements and used a k-ω turbulence closure with a Low-Reynolds-Number correction. Measured bed surface and water surface profiles provided the physical boundary of the numerical domain. The inlets and outlets of the surface flow models were treated as periodic boundaries with the periodic pressure gradient defined by the energy slope. The water surface was modeled as a symmetry boundary and the bed surface as a no-slip wall boundary. Residual error for continuity, x-velocity, y-velocity, k, and ω was set to less than 1×10^{-6} for convergence. The overall CFD modeling approach was validated against the pressure measurements provided by Fehlman (1985). Excellent agreement between the simulated and measured bed-pressures, over a broad range of discharges and energy head, gave us a high degree of confidence that our modeling approach was robust, accurate, and not overly sensitive to the applied boundary conditions (Reeder, Quick, Farrell, Benner, Feris, & Tonina, 2018).

Hyporheic flowlines (red and green lines, Figure 2) and the associated residence times (τ) were quantified using the models of Marzadri (Marzadri, Tonina, McKean, et al., 2014) and GMS ModFlow (Aquaveo, LLC, Provo, Utah). The Marzadri model provides a semianalytical solution to the groundwater flow equations and ModFlow provides a numerical solution. The two approaches were used as a crosscheck and to utilize the visual presentation of GMS ModFlow. Calculated residence times were calibrated (by adjusting hydraulic conductivity) against measured residence times from a post experiment salt pulse injection at the end of Flume 2. Salt solution was constantly added into the head box of the flume for approximately 30 min to raise the surface water salt concentration to approximately 100 mmol/L. Electrical conductivity was measured with electrical conductivity sensors placed at a subset of the sampling ports (purple dots, Figure 2). Measurements were recorded every 5 min for approximately 3 days using Model CR1000 data loggers (Campbell Scientific, Logan, UT, USA). Residence times were calculated from breakthrough curves at 9 locations in a 70 cm dune and 20 locations in a 100 cm dune (Reeder, Quick, Farrell, Benner, Feris, & Tonina, 2018).

2.4. Flowlines and Chemical Concentration Profiles

The measured N_2O concentration data were krigged and gridded (Surfer ® Version 10, Golden Software, Inc., Golden CO) to create N_2O concentration maps for each dune. The concentration profile for the C70 dune on Day 91 of the Flume 2 experiment is shown in Figure 2. The kriging operation creates a regular grid of X-Y locations and assigns an N_2O concentration that is interpolated from the measured values, to each location. The interpolation is constrained such that the measured values are not altered. For each of the dunes, flowlines (red and green traces, Figure 2) were calculated from the pressure profile for that particular dune. Those flowlines were mapped onto the associated N_2O concentration profile. The data stream for flowline traces consist of a series of X-Y locations with a residence time at each location. For each flowline, from these co-mapped data sets, we extracted a data string of paired residence time and the N_2O concentration (τ, [N_2O]). The two profiles in Figure 3 are representative examples of individual flowline N_2O concentration profiles presented as a function of residence time. With these data, we can parse the chemical activity in the HZ to a fine level. For instance, we can locate the residence time and position of the peak of net production of N_2O along the flowline as well as the N_2O concentration and residence time at flowline exit. Additionally, by calculating an exponential fit to the rising and falling limbs of the [N_2O] versus τ profiles, we can calculate the apparent first-order reaction kinetics for N_2O production and consumption, respectively. It is likely that production and consumption are happening simultaneously and, thus, calculated rates should be viewed as apparent as opposed to thermodynamic. DO and other chemical constituents can be treated in a similar manner. We used the same procedure, with τ versus [DO] data streams, to calculate the rate constant of metabolic DO consumption (K_{DO}) for all flowlines (Reeder, Quick, Farrell, Benner, Feris, & Tonina, 2018).

2.5. Calculation Methodologies

2.5.1. Distributed K_{DO} Transform

Following previous approaches (Ocampo et al., 2006), we define a Damköhler-type transformation that scales the residence times (τ) along each of the individual flowlines by a characteristic reaction rate for each of the flowlines (Marzadri et al., 2011; Zarnetske et al., 2011a; Zarnetske et al., 2012). We used K_{DO}, the rate constant

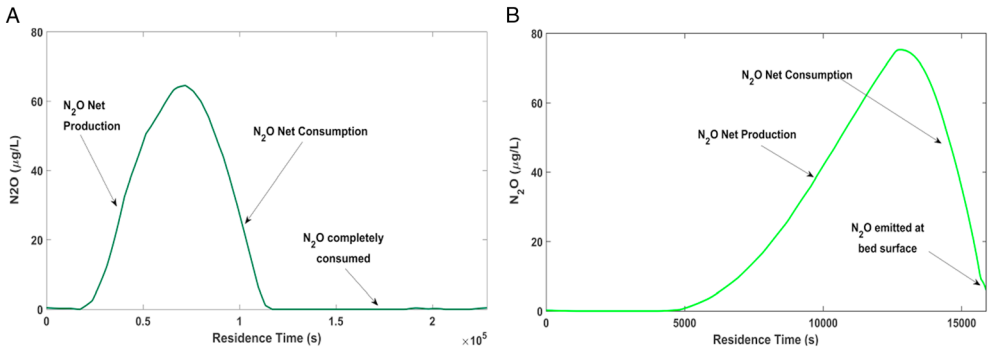

Figure 3. N_2O concentration versus τ profiles for two different flowlines from the Channel C, 70 cm dune on Day 91 of the Flume 2 experiment. (a) Illustrates a long flowline (dark green trace, Figure 2) in which N_2O is consumed to below the surface water concentration. This flowline serves as a sink for N_2O. (b) Illustrates an intermediate length flowline (light green trace, Figure 2) whose exit concentration is above the surface water concentration. This flowline is a source of N_2O. Please note the different time scales on the two graphs. In both cases, the time scale is the full amount of time that a parcel of water traveling along that flowline spends in the HZ. N_2O = nitrous oxide.

for the metabolic consumption of DO. The transformed residence times are designated as $\tilde{\tau}$, and the transform is calculated by

$$\tilde{\tau}_i = \tau_i \cdot K_{DOi}, \tag{1}$$

where $\tilde{\tau}_i$ is the collection of transformed residence times (τ) from flowline (i) and K_{DOi} is the DO consumption rate constant for flowline (i). The $\tilde{\tau}$ transform is calculated for all flowlines using individual K_{DO} values that have been calculated for each of the flowlines.

In Reeder, Quick, Farrell, Benner, Feris, and Tonina (2018), we showed that, for dune-like bedforms, K_{DO} values are lognormally distributed and that flowline K_{DO} values can be calculated from the mean K_{DO}, $\overline{K}_{DO}$, and the standard deviation, σ_{KDO}. They can be estimated by using the log transform variable, $Y = \ln(K_{DO})$, the log transform mean, μ_Y, and the standard deviation, σ_Y, from the inverse normal distribution:

$$K_{DO} = \exp\left(F^{-1}(X^*|\mu_Y, \sigma_Y)\right), \tag{2}$$

where

$$F(Y|\mu_Y, \sigma_Y) = \frac{1}{\sigma_Y\sqrt{2\pi}} \int_o^Y e^{\left\{\frac{-(\ln\xi - \mu_Y)^2}{2\,\sigma_Y^2}\right\}} d\xi, \tag{3}$$

where ξ is a dummy variable of integration and X^* is the dimensionless, horizontal distance along the upstream downwelling face of the bedform, defined as

$$X^* = x/\lambda', \tag{4}$$

with λ' as the horizontal length of the downwelling face of the bedform. In a triangular dune, λ' is simply the streamwise distance from the trough to the crest of the dune such that $X^* = 0$ at the trough (position 0 m in Figure 2) and 1 at the crest (position 0.5 m in Figure 2). More simply, the flowline K_{DO} values can be calculated in Excel or Matlab using the expression

$$K_{DOi} = \exp(norminv(X^*, \mu_Y, \sigma_Y). \tag{5}$$

2.5.2. Mean K_{DO} Transform, $\overline{K}_{DO}$

Alternatively, the $\tilde{\tau}$ transform can be calculated using the mean K_{DO} of a particular bedform for all flowlines in that bedform. This is less precise than the distributed transform but it may be useful in some situations. For this approach, the transform takes the form

$$\tilde{\tau}_i = \tau_i \; x \; \overline{K}_{DO}. \tag{6}$$

2.5.3. N_2O Flux Calculations

N_2O flux for each flowline was calculated as

$$f_i = \begin{cases} 0, & \widetilde{\tau}_{up(i)} < 0.54 \\ v_{dw(i)} \, x \, A_{dw(i)} \, x \, [N_2O]_{up}, & 0.54 \leq \widetilde{\tau}_{up(i)} \leq 4.4 \\ v_{dw(i)} \, x \, A_{dw(i)} \, x \, \left([N_2O]_{min} - [N_2O]_{surf}\right), & \widetilde{\tau}_{up(i)} > 4.4 \end{cases}, \quad (7)$$

where i refers to the ith flowline such that f_i is the flux from the ith flowline, $v_{dw(i)}$ is its downwelling velocity, $A_{dw(i)}$ is its downwelling surface area, $[N_2O]_{up}$ is its N_2O concentration as the ith flowline exits the HZ, $[N_2O]_{surf}$ is the N_2O concentration of the surface water, and $[N_2O]_{min}$ is the minimum N_2O concentration along flowline (i). Total flux from a bedform is calculated by summing the fluxes from all flowlines. The derivation for the thresholds ($\tilde{\tau}_{up}$ = 0.54 and 4.4) is presented in section 3.2.2.

3. Results and Discussion

3.1. N_2O Production and Consumption Profiles

The blue profiles in Figure 2 show the krigged N_2O concentrations for the C70 on Day 91 of the Flume 2 experiment. Compared to the other dunes, the C70 dune experienced higher levels of bioactivity, and as a result, its profile map is somewhat more spatially extensive and continuous than the other dunes. Nonetheless, the morphology, extent, and location of all the N_2O plumes is quite similar to the C70 profile. Residence time versus N_2O concentration profiles (τ, [N_2O]) were extracted for all flowlines that intersected the various N_2O plumes. Two representative profiles are shown in Figure 3. The concentration profile in Figure 3a is from a long flowline (dark green flowline, Figure 2). The rising limb of the profile traces production of N_2O and the falling limb is consumption. The N_2O concentration at the entry point of the flowline was 0.55 μg/L and peaked at about 65 μg/L. All N_2O was consumed before the flowline exited the HZ. This flowline functions as a sink of N_2O. The concentration profile in Figure 3b is for an intermediate length flowline. As with the long flowline (Figure 3a), both production and consumption are occurring along this flowline. However, this flowline exits the bed before all N_2O is consumed and, at least on this date, was acting as a source of N_2O to the surface flow.

The N_2O concentration profiles for all flowlines from all dunes are shown in Figure 4. Within this collection of N_2O concentration profiles, there is a wide range of production and consumption responses. From flowline to flowline, the initiation of production and peak production occurs at different points in (residence) time. The magnitude of the peak and terminal concentrations vary by flowline. The apparently tight grouping of the profiles is somewhat deceptive. The large number of data points (>100,000) and the inherent similarity between the experiments tend to obscure the broad diversity of responses. When the flowlines are evaluated against the tendency to emit N_2O, it is difficult to identify a concise range of residence times (τ) and flowlines that have a high probability to emit N_2O. The concentration data in this format is not particularly useful as a predictive tool.

3.2. Scaling and Classifying the N_2O Profiles

3.2.1. Distributed (Lognormal) Transform

Most of the variability among the concentration profiles in Figure 4 comes from variability between flowlines as opposed to variability between dunes. Reeder, Quick, Farrell, Benner, Feris, and Tonina (2018) showed that, when evaluated at the flowline level, the metabolic DO consumption rate, expressed as K_{DO}, is a linear function of the downwelling velocity of that flowline. Flowline downwelling velocities, for a bedform, are lognormally distributed and, thus, so too are the values expressed by K_{DO} indicating that biological activity within a dune is likely to be lognormally distributed. Based upon these observations, it seemed a reasonable possibility that scaling the residence times (τ) by a characteristic reaction rate would yield a nondimensional residence time that would tend to group similar events together. To test this idea, we multiplied the flowline residence times (τ (s)) by the DO consumption rate constant (K_{DO} (1/s)) for each flowline. K_{DO} values were calculated from the lognormal distribution of K_{DO} values for the dune in which a particular flowline resided. We designate the transformed, nondimensional residence times as $\tilde{\tau}$. The results of the $\tilde{\tau}$ transform are shown in Figure 5. N_2O production for the majority of the profiles initiates within relatively small range of $\tilde{\tau}$ values (~0.5 to 1). The N_2O concentration peaks are reasonably well aligned, as are the falling limbs of the profiles,

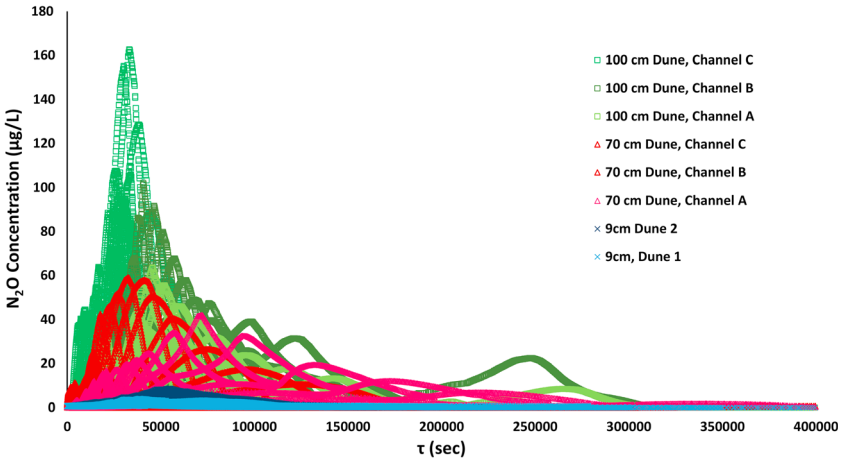

Figure 4. N_2O concentration profiles for all flowlines and all dunes considered in this experiment (70 cm dune [Channels A, B, and C], 100 cm dune [Channels A, B, and C], and 9 cm dune 1 and 9 cm dune 2). The 9 cm dune data are from Day 112 of the Flume 1 experiment. All other data is from Day 91 of the Flume 2 experiment. The apparently tight grouping of the profiles is somewhat deceptive. The large number of data points (>100,000) and the inherent similarity between the experiments tends to obscure the natural diversity of the responses. Note that some of the profiles exhibit a secondary peak. These peaks are probably anomalous and likely due to divergence between our modeled flowlines (uniform arcs based on the model assumption of homogeneity) and the actual physical flow paths that wander due to physical heterogeneity (e.g., Tonina et al., 2016). In some cases, the modeled flowlines do not perfectly track the paths of the physical flowlines and are likely to cross physical paths that have a different N_2O production and consumption history. The krigging process may also account for some of the secondary peaks. N_2O = nitrous oxide.

indicating consumption. Collectively, these profiles potentially define a concise range of $\tilde{\tau}$ values that encompass N_2O production and consumption for a broad range of bedforms.

To generalize the collective data shown in Figure 5 and to define beginning and ending points for N_2O production and consumption as well as the peak production point, we calculated a mean profile for the collective flowline data. However, the various dunes and their flowlines present a broad range of amplitudes for the N_2O concentration profiles. We were concerned that the high amplitude profiles would dominate and bias the mean profile. To test this concern, we calculated the mean profile using two different approaches. In the first approach, the N_2O concentrations (Figure 5) were binned by their $\tilde{\tau}$ values, with each bin having a width of 0.1 (number of observations in each bin was ~1,000). All N_2O values in each bin were averaged and plotted to the midpoint of the bin (orange line, Figure 6). In the second approach, the amplitudes of all flowlines were normalized to the maximum values of each of the individual flowlines. Thus transformed, each of the normalized flowlines exhibited values that ranged from 0 to 1. The normalized values were binned, averaged, and plotted in the same manner as used in the first approach (blue line, Figure 6). We calculated the mean and standard deviation using the expressions

$$\bar{\tilde{\tau}} = \frac{1}{\sum C_i} \sum_{1}^{n} c_i \cdot \tilde{\tau}_i \tag{8}$$

for the mean and

$$\sigma^2 = \frac{1}{\sum C_i} \sum_{1}^{n} c_i \cdot \left(\tilde{\tau}_i - \bar{\tilde{\tau}}\right)^2 \tag{9}$$

for the variance. The mean and standard deviation (square root of the variance) for the non-normalized data were 1.82 and 0.64, respectively. For the normalized data, the mean and standard deviation were 1.65 and 0.91, respectively. For both approaches, the mean and standard deviation were quite similar, suggesting that differing amplitudes among the flowlines was not overly biasing to the result. Using the non-normalized data, we define lower and upper boundaries for N_2O production and consumption. The lower boundary for production is defined as the mean (1.82) minus two standard deviations giving a lower limit of N_2O production at $\tilde{\tau}$ = 0.54 (gray vertical line, Figures 5 and 6). The upper limit of consumption is defined as the mean (1.82)

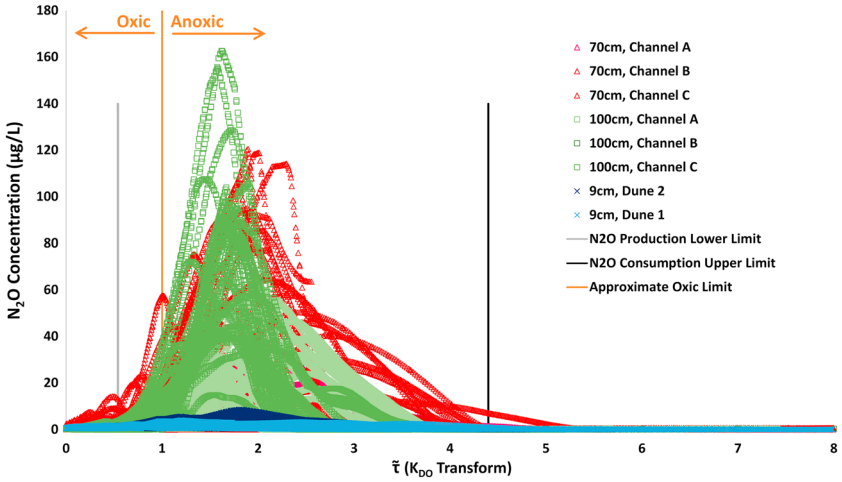

Figure 5. N_2O concentration profiles for all flowlines and all dunes plotted against the nondimensional residence time, $\tilde{\tau}$. In this case, the tight grouping of the concentration profiles is a result of the $\tilde{\tau}$ transform. This provides a useful tool for predicting N_2O production and consumption. For this chart, each flowline was transformed using the K_{DO} value calculated for that specific flowline. N_2O = nitrous oxide.

plus four standard deviations giving an upper limit of production at $\tilde{\tau} = 4.4$ (black vertical line, Figures 5 and 6). The reason for unbalanced use of standard deviations is the relatively long tail on the consumption side of the profile. This unbalanced approach creates limits that match well to a threshold line (black, horizontal, dashed line, Figure 6) set at $[N_2O] = 0.65$ µg/L, just above surface water equilibrium concentration. The meaning of these limits is that, on average, for any particular flowline, N_2O production will be initiated at $\tilde{\tau} = 0.54$, the N_2O concentration will peak at $\tilde{\tau} = 1.8$ and, if the flowline is long enough, all N_2O will be consumed by $\tilde{\tau} = 4.4$. The $\tilde{\tau}_{up}$ is the transformed residence time at the point where a flowline exits the bed and reenters the surface water. If a flowline has a $\tilde{\tau}_{up}$ between $\tilde{\tau} = 0.54$ and $\tilde{\tau} = 4.4$, it has the potential to emit N_2O. The physical events tied to these boundaries are, at the lower boundary ($\tilde{\tau} = 0.54$), the consumption of DO to a sub oxic state (though not necessarily anoxic), causing the initiation of metabolic consumption of reactive nitrogen compounds and, at the upper boundary ($\tilde{\tau} = 4.4$), the completion of the denitrification reaction sequence.

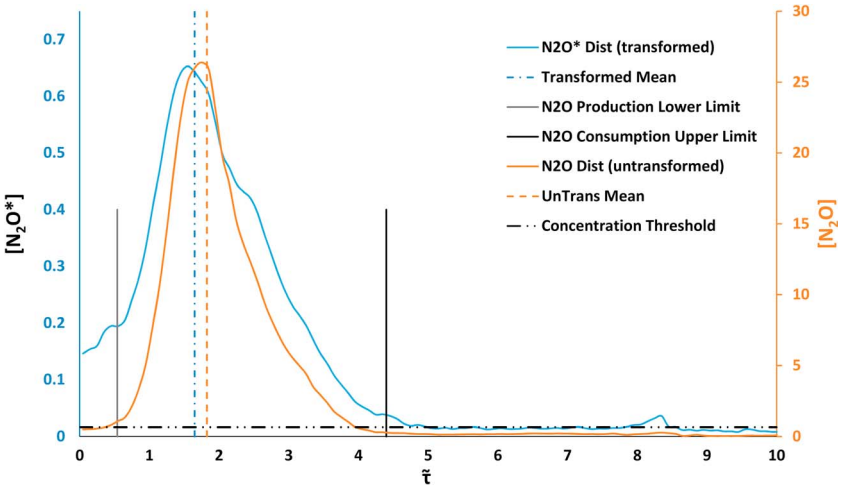

Figure 6. Mean N_2O concentration profiles (for all dunes) by two different approaches. In both approaches, N_2O concentration values were binned by $\tilde{\tau}$, with each bin having a width of 0.1. All N_2O values in each bin were averaged and plotted to the midpoint of the bin. In Approach 1 (orange line), averages were calculated against the raw (un-normalized data). In Approach 2 (blue line), the N_2O values for all flowlines were normalized by the peak N_2O value for each of the flowlines. N_2O = nitrous oxide.

Interestingly, the production of N_2O spans $\tilde{\tau}_{up}$ pore water conditions between bulk aerobic and anaerobic and peaks at times or locations well in anoxic conditions ($\tilde{\tau}_{up}$ = 1.8). Values of $\tilde{\tau}_{up}$ less than 1 indicate that the bulk pore water has DO concentrations higher than the threshold concentration for anaerobic conditions, suggesting that N_2O production consistently and systematically starts in the oxic zone of the HZ. This production could be due to different mechanisms that may include denitrification in microanoxic zones, nitrification (oxidation of ammonia to nitrite and nitrate, *Hydroxylamine Oxidation*) and chemo-denitrification (Otte et al., 1996, 1999; Schreiber et al., 2012). However, the highest N_2O concentrations occur in the anoxic zone of the HZ, suggesting that denitrification is probably the main mechanism producing N_2O in this environment.

3.2.2. Adapting to Surface DO and Temperatures that Vary From the Reference Conditions

For our experiments, surface water temperatures were substantially constant at around 17 °C, as were DO concentrations at around 8.5 mg/L. The N_2O production and consumption limits are referenced to those conditions. It is possible that a significant shift to those reference conditions, particularly the surface water DO concentration, could cause a shift to those limits. If, for example, the surface water DO concentration were 10 mg/L and all other factors were held the same, the initiation of denitrification would be delayed as compared to the 8.5 mg/L condition. This may cause the limits of production and consumption to shift to higher values of $\tilde{\tau}$. To accommodate significant variations in DO concentration and following the work of Marzadri et al. (2011), we suggest that $\tilde{\tau}$ transform (from equation (1)) could be modified to the following form:

$$\tilde{\tau} = \frac{\tau \cdot K_{DO}}{\ln \frac{[DO]_s}{[DO]_{lim}}}, \tag{10}$$

where $[DO]_s$ is the surface water DO concentration and $[DO]_{lim}$ is the limiting concentration for aerobic activities, typically 2 mg/L, and the reaction rate constant could be adjusted by the local water temperature, T, with an Arrhenius equation like

$$K_{DO\ (T)} = K_{DO\ (T=20C)} \cdot \varphi_{K_{DO}}^{(T-20)}, \tag{11}$$

with the temperature coefficient for respiration of $\varphi_{K_{DO}} = 1.047$ (Marzadri et al., 2013).

3.2.3. Single-Value Transform

Recognizing that it is difficult to obtain K_{DO} values for individual flowlines, it is also possible to transform the residence time (τ) values for a bedform using a single value of K_{DO}. This might be single measured value for a particular bedform or the mean of a few measured values. While this transform approach is somewhat easier than the lognormally distributed transform, the distribution of the transformed curves is wider and more dispersed, and as a result, this approach is less precise.

3.3. Modeling N_2O Emissions

3.3.1. Identifying Potential Emissions

Potentially, the $\tilde{\tau}$ transformation allows us to extend our findings to virtually any bedform. More research needs to be done to define clearly just how widely these results can be applied. However, the consistency and repeatability of the responses across bedform geometries, bedform replicates, and the two experiments suggest that, if the residence times within the HZ are known, the $\tilde{\tau}_{up}$ values can be used to evaluate the potential of a particular bedform or for a collection of bedforms to produce and emit N_2O across a broad range of bed morphologies. Flowlines that have a $\tilde{\tau}_{up}$ value of less than 0.54 are too short to produce N_2O. These flowlines will likely remain relatively oxic and are unlikely to have a significant impact on the overall nitrogen chemistry of the stream or HZ. Flowlines that have a $\tilde{\tau}_{up}$ value that is greater than 4.4 will produce N_2O but, for the most part, all N_2O will have been consumed before the flowline exits the bed. These flowlines have the potential to act as a sink of N_2O by consuming it to concentrations below that of the surface water. Flowlines that have a $\tilde{\tau}_{up}$ between those two limits have a significant potential to produce and emit N_2O. The above classifications all assume that the concentration of nitrate and/or ammonium in the surface water and the sediments is sufficient to produce significant levels of nitrification and denitrification. It is also assumed that the bed sediments contain sufficient levels of bioavailable carbon to support the anaerobic metabolic activities that drive the denitrification reaction sequence.

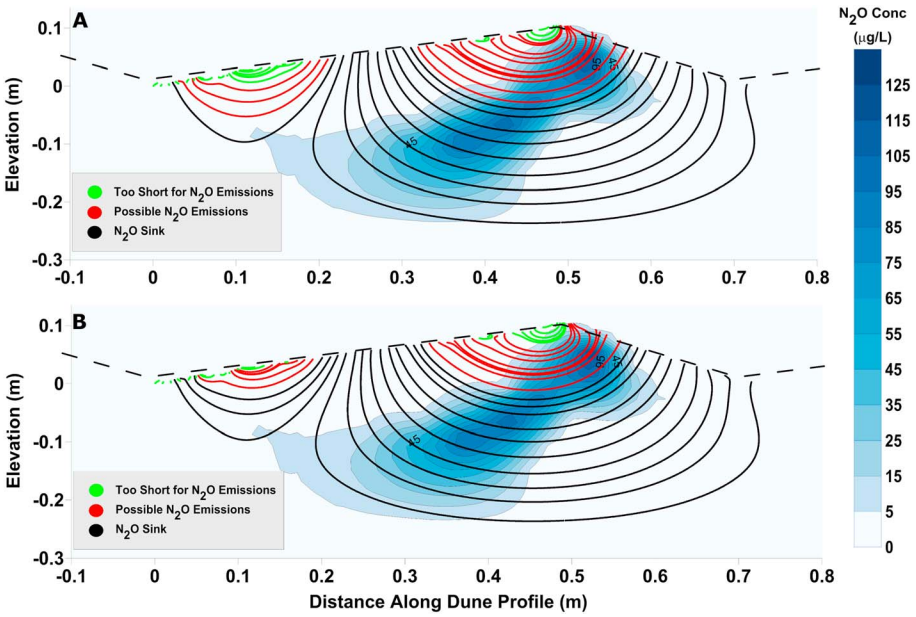

Figure 7. Flowlines are colored by their tendency to produce and emit N_2O. Green lines ($\tilde{\tau}_{up} < 0.54$) are too short to produce or emit. Black lines ($\tilde{\tau}_{up} > 4.4$) are too long to emit N_2O and may act as a sink. Red lines ($0.54 < \tilde{\tau}_{up} < 4.4$) have the potential to produce and emit N_2O. In (a), the $\tilde{\tau}$ values were calculated using the lognormally distributed K_{DO} values for each flowline. In (b), the $\tilde{\tau}$ values were calculated using the mean K_{DO} value for the dune—one K_{DO} value was used for all flowlines. The dune represented in this figure is the Channel C, 70 cm dune from Flume 2.

This classification approach for identifying N_2O-emitting flowlines is illustrated in Figure 7. The green lines in this figure are flowlines that have been identified as being too short ($\tilde{\tau}_{up} < 0.54$) to produce and emit N_2O. The black lines are flowlines that are identified as being too long ($\tilde{\tau}_{up} > 4.4$). The red lines are the flowlines that have the potential to emit N_2O. The two panels compare the flowline classifications using the distributed and single-value K_{DO} transform techniques. In Figure 7a, the $\tilde{\tau}_{up}$ values and flowline classifications are derived from the (lognormally) distributed K_{DO} transform—all flowlines are transformed by a K_{DO} value that is specific to that flowline. In Figure 7b, all flowlines were transformed by the single-value (mean) K_{DO} transform using the mean K_{DO} value for that dune. The same $\tilde{\tau}_{up}$ limits were applied to the flowlines from both transforms and it is interesting to note, at least for this bedform, that the two classifications are remarkably similar. This is a bit surprising given the broad dispersion of the mean K_{DO} transform relative to the distributed K_{DO} transform. The mean K_{DO} transform classifies fewer flowlines as potential emitters of N_2O, but, nonetheless, gives a useful estimation of which flowlines have the potential to emit. The idea of *potential to emit* needs to be stressed. Not every red flowlines, from either classification scheme, is certain to emit N_2O. While our model focuses on the hydraulic controls over biological processes, it is clear that, for instance, nitrate loading in the stream water or the state of the biological communities at a point in time will have an impact on the final chemistry that exits a flowline. The model defines an upper limit on what is possible based upon the ambient chemistry and the stream hydraulics. We know, for instance, that the flowlines on the left side of the dune near the upstream trough (between $x = 0$ and 0.2, Figure 7), which have been classified as potential emitters, actually do not emit N_2O. On the date captured by this figure, that area was oxic (Reeder, Quick, Farrell, Benner, Feris, & Tonina, 2018) and, thus, anaerobic respiration and denitrification processes were not active. The power of classifying flowlines is twofold. First, this approach can be used in natural streams, in which the hydraulics and hyporheic residence times are known, to connect measured N_2O emissions to the source locations. Second, if the analysis is done prior to restoration or experimental work, it can be used to improve the effectiveness of those efforts.

If it is only desired to estimate the portion of the flowlines from a bedform or collection of bedforms that have the potential to emit N_2O, then a procedure somewhat simpler than mapping the flowlines can be used. A cumulative density function (CDF) of the $\tilde{\tau}_{up}$ values can be constructed (Figure 8). The portion of the CDF that falls between the lower and upper limits for N_2O production and consumption will be the portion of the

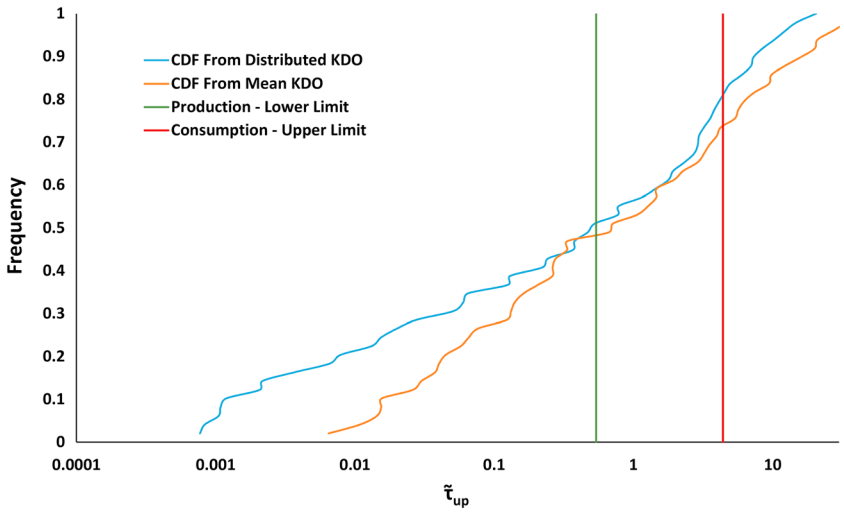

Figure 8. CDFs of the $\tilde{\tau}_{up}$ values for the flowlines in the Channel C, 70 cm dune on Day 91. The blue line is the CDF for $\tilde{\tau}$ values calculated using the distributed (individual) K_{DO} values and the orange line is the CDF of $\tilde{\tau}$ values calculated using the mean K_{DO}. CDF = cumulative density function.

flowlines that have the potential to emit N_2O. The two CDFs presented in Figure 8 are from the same dune (C70, Day 91) and are the CDFs for the flowline classification schemes shown in Figure 7. Consistent with the flowline classifications in Figure 7, the CDF for the distributed K_{DO} transform (blue line) classifies approximately 34% of the flowlines as potential emitters, while the CDF for the mean K_{DO} transform (orange line) nominates only 26% as potential emitters. This approach does not identify which flowlines or bedforms have the potential to emit.

3.3.2. Scaling the Model

Whereas the proposed method does not predict the magnitude of N_2O emission from the HZ, it does identify the flowlines that may produce or remove N_2O concentrations at the upwelling zones. Additionally, it provides a powerful method to upscale processes at the local flowline scale to bedform and eventually to reach scale production of N_2O emissions once the residence time distribution within the HZ is known. Presently, available predictive models, with their own limitations, for the distribution of hyporheic residence time for streams are limited to dune-like (Elliott & Brooks, 1997) and pool-riffle (Marzadri et al., 2011) morphologies. By applying the analysis reported in the previous section, the method quantifies the percent of flowlines with the potential to emit N_2O. The constrains on $\tilde{\tau}_{up}$ can allow quantifying whether a reach can remove or emit N_2O. The latter will be true if all $\tilde{\tau}_{up}$ are longer than 4.4.

In idealized streambed conditions, (perfect dune-like and pool-riffle bedforms) this also implies mapping the sources or sinks of N_2O over the streambed. For other bedforms, for which predictive models of the hyporheic residence time are not available, the process may require to develop a hyporheic model supported by stream and river bathymetry and hydraulic conductivity distribution. Whereas the former is potentially at reach with the advances in remote sensing techniques, including structure from motion photogrammetry (Dietrich, 2017; Javernick et al., 2014; Storlazzi et al., 2016; Woodget et al., 2015) and bathymetric light detection and ranging (Hilldale and Raff, 2008; Kinzel et al., 2013), as applied by Benjankar et al. (2016), the latter is more challenging as mapping hydraulic conductivity is still difficult and there is not yet a viable field methodology. The current approach is to apply stochastic analysis by considering the physical values (e.g., emissions and hyporheic residence time) as stochastic variables and assume that their spatial variability behave as a stochastic variability at the reach scale, such that ensemble analysis can provide reach scale values as proposed by Tonina et al. (2016).

3.3.3. Estimating N_2O Fluxes

In cases where the N_2O concentration profiles and flowline residence times are known or can be modeled, the $\tilde{\tau}$ can be used to refine estimations of N_2O emissions. This can be easily accomplished by coding equation (7) and summing the fluxes from the individual flowlines. Using this procedure and the classifications from the distributed K_{DO} transform, the net fluxes were calculated for all of dunes examined in this

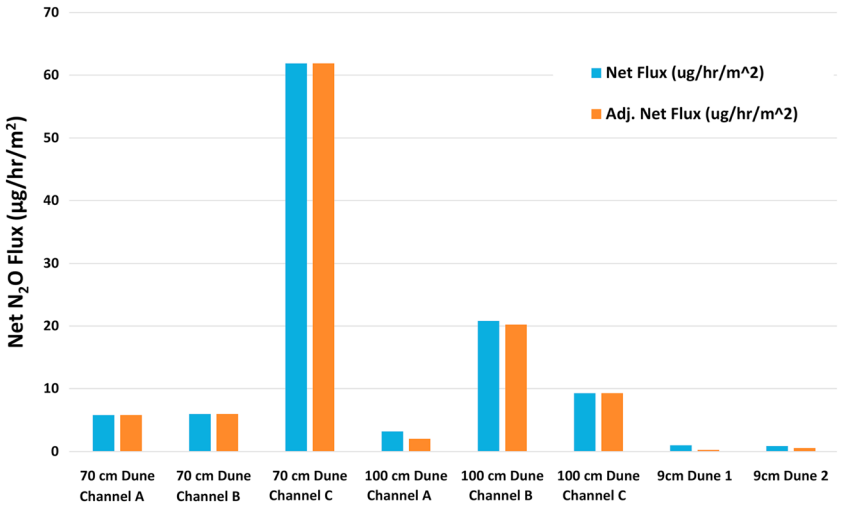

Figure 9. Net N_2O flux from each dune. All calculations are based upon the distributed K_{DO} transform. Adjusted flux values are based upon the observation that some of the flowlines that were included in the *possible emissions* bin exhibited no N_2O concentrations that exceeded the surface concentration by at least 5%. For these flowlines, the net flux has been set to zero. N_2O = nitrous oxide.

experiment (Figure 9). The blue bars represent the flux estimations, with all of the flowline flux calculations based strictly upon the $\tilde{\tau}_{up}$ classifications in equation (7). However, not all flowlines in the *possible emissions* class will emit N_2O. In our data sets, it was observed that some of the flowlines included in that class did not exhibit a significant level of N_2O production. For possible emissions flowlines whose peak N_2O concentrations did not exceed the surface concentration by at least 5%, the effluent flux was set to zero. The result of the adjustment is shown by the orange bars in Figure 9. For the 70 cm dunes, the difference between the adjusted and unadjusted fluxes was negligible. For the 100 cm dune and the 9 cm dunes, the difference was slightly more than that of the 70 cm dunes but still quite modest. Overall, the upper and lower $\tilde{\tau}$ limits seem to be correctly placed and the potential error in the model is small. The dunes in the Flume 2 experiment (Channels A, B, and C, 70 and 100 cm dunes) exhibited significantly higher N_2O emissions than the Flume 1 experiment (9 cm dune). The higher emissions from Flume 2 are consistent with the higher nitrate loading in that experiment. These flux estimations also point up the importance of experimental replicates in biochemical experiments. In Flume 2, the N_2O concentrations and the estimated N_2O fluxes exhibited significant variability across the replicates, both for the 70 and 100 cm dunes. This is not particularly surprising. If one were to imagine multiple biological systems, all with similar starting points, over time it would be expected that these systems would exhibit a range of responses that are likely driven by relatively small differences between the individual systems. Given this apparently inherent variability, estimations based upon measurements from a single source and extrapolated to a larger context might be poorly representative of the larger context. For instance, if we were to have made an estimate of the flux from all of our dunes base solely upon the C70 measurements, we would have likely overstated the overall flux. The specific reason(s) for the high flux value (and high N_2O concentrations) for dune C70 are not explained by any specific observation that we can offer at this time.

The spatial distribution of N_2O emissions from the HZ has not been previously described. The actual behavior may be a bit counterintuitive. Figure 10 shows the spatial distribution, in the dimensionless coordinate X^*, of N_2O emissions from all dunes considered in this study. The brown line at the bottom represents a simplified dune-surface profile. For this diagram, emissions were assigned to the horizontal dimensionless position (X^*) of entry point of the flowline into the bed for which the emissions were calculated. This was done to highlight which flowlines and portions of the bedform are responsible for specific outcomes. Actual emissions occur downstream of the crest (Figure 10). Net N_2O consumption (negative emissions) occurs mostly along the flowlines that enter the bed between $X^* = 0.2$ and $X^* = 0.55$. Most N_2O sourcing occurs between $X^* = 0.55$ and $X^* = 1$ (the dune crest). There is a generally rising trend in N_2O emissions from flowlines that enter at $X^* = 0.55$ to those that enter at $X^* = 1$, with the strongest emissions coming from flowlines that enter

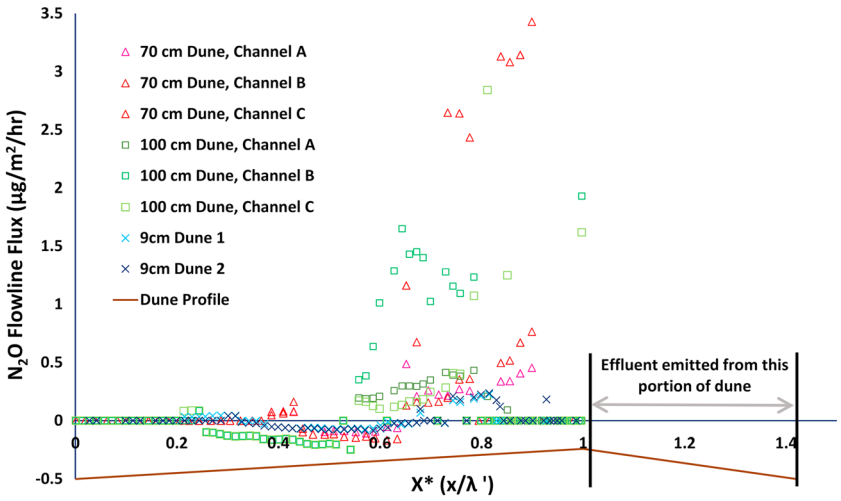

Figure 10. Spatial distribution of N_2O flux values from all dunes in the two experiments. The brown line at the bottom of the chart represents a generalized dune surface profile. Note that the horizontal distance along the dune has been transformed to a nondimensional distance, X^* ($X^* = x \cdot \lambda'$). Where x is the untransformed horizontal distance along the dune profile and λ' is the length of the dune from trough to crest. The fluxes are assigned to the entry point of the flowline—the actual emissions occur downstream of the dune crest N_2O sinking occurs mainly between $X^* = 0.2$ and $X^* = 0.55$. Most N_2O sourcing occurs between $X^* = 0.55$ and $X^* = 1.0$ (dune crest). There is a generally rising trend in flowline flux from $X^* = 0.55$ to $X^* = 1.0$, with the strongest emissions between 0.8 and 0.9. N_2O = nitrous oxide.

between $X^* = 0.8$ and $X^* = 0.9$. It is not intuitively obvious that the maximum emissions should come from flowlines that enter the bed near the crest of the dune. This is not where the highest N_2O concentrations are observed. However, N_2O emissions are the product of the velocity along the flowline and the N_2O concentration at flowline exit. Concentrations vary by a factor of three or four, whereas downwelling velocities vary by an order of magnitude (Reeder, Quick, Farrell, Benner, Feris, & Tonina, 2018). Thus, peak production is a result of the synergy between strong flowline flux and N_2O concentration. This also suggests that while anaerobic denitrification may produce the highest N_2O concentrations within the bulk of the HZ (Figures 5 and 7), the processes within the oxic zone with $\tilde{\tau}_{up}$ values from 0.5 to 1 because of their high velocities (flowpath near the crest; Figures 7 and 10) may be the main sources of N_2O fluxes to the stream water. This could potentially explain the lower sensitivity of a Damköhler number based on DO consumption time scale (Marzadri, Tonina, Bellin, et al., 2014) than that based on denitrification time scale (Marzadri et al., 2017) to predict N_2O emissions at the reach scale, because denitrification time scale will be the limiting factor rather than DO.

4. Conclusions

Our results show that only a portion of the flowlines through the HZ are likely to emit N_2O, while others will sink N_2O to below instream concentrations. The primary factors that determine whether a particular flowline will emit N_2O are the residence time and biological activity level (reflected by K_{DO}) along that flowline, with the latter being influenced by the distribution and reactivity of organic carbon and denitrifying bacterial communities. Our results support and quantify the conceptual model proposed by Quick et al. (2016) that short or long flowlines are unlikely to emit N_2O. Short flowlines may have not started denitrification, thus will not produce N_2O but pass through the dissolved concentration from the flow. For long flowlines, the denitrification reaction sequence will likely be carried to completion and the primary effluent from those flowlines will be nitrogen gas (N_2), assuming reactive carbon is not limiting. Long flowlines may act as a sink by consuming N_2O to below the concentration of the surface water that entered the HZ. Because reaction rates (DO consumption, N_2O production, and N_2O consumption) are variable from flowline to flowline, residence time, by itself, is not an adequate predictor of N_2O emissions. However, as a general predictor of N_2O emissions for most bedforms, we propose to transform the residence times (τ (s)), for the individual flowlines, to a nondimensional, Damköhler number, $\tilde{\tau}$, by multiplying the τ values by a characteristic reaction rate for that

flowline, in this case K_{DO} (1/s) ($\tilde{\tau} = \tau \cdot K_{DO}$). Through the $\tilde{\tau}$ transform, we can predict the locations and portions of a bedform that will act as source or sink for N_2O. Our results suggest that the initiation of denitrification occurs at values of $\tilde{\tau} > 0.54$. Peak N_2O production occurs at $\tilde{\tau} \cong 1.8$. N_2O consumption is complete at values of $\tilde{\tau} > 4.4$. Flowlines for which $\tilde{\tau}_{up}$ (the nondimensional residence time, $\tilde{\tau}$, at which a flowline exits back into the surface water) is between 0.54 and 4.4 will produce and potentially emit N_2O. An adequate estimation of $\tilde{\tau}$ can be calculated by multiplying the τ values for all flowlines in a bedform by the mean K_{DO} value for that bedform. However, if the mean K_{DO} value and standard deviation are known, or can be estimated, individual K_{DO} values can be calculated for each flowline refining the predictive power of the $\tilde{\tau}$ transform. K_{DO} values are associated with hyporheic downwelling flows and are lognormally distributed for dune-like bedforms. In either case, mean K_{DO} or distributed K_{DO}, a CDF of the $\tilde{\tau}_{up}$ values for all flowlines in a bedform (or multiple bedforms) can be constructed and the portion between 0.54 and 4.4 is a direct estimate of flowlines that have the potential of emitting N_2O. These constrains on the hyporheic residence time CFD allows upscaling the results to other bedforms and to reach scale processes as long as there is a model for the hyporheic hydraulics like that for dune-like or pool-riffle.

The range of $\tilde{\tau}$ spans both aerobic ($\tilde{\tau} < 1$) and anaerobic ($\tilde{\tau} > 1$) bulk pore water conditions, indicating that N_2O production systematically starts in the HZ with bulk pore water oxic conditions. Our results show that for a given nutrient load, hyporheic hydraulics and thus stream flow/bedform interactions exert control on biological activity and are, at a significant level, responsible for hot spots of high production rates of transformed products occur. In fact, flowlines with high downwelling flow velocities identify or cause the biogeochemical hot spots. Most N_2O emitted from a dune-like bedform is produced from hyporheic flows that enter the bed within a narrow downwelling band just upstream of the dune crest ($0.8 < X^* < 0.9$), where downwelling velocities are high. This highlights our suggestion that hyporheic hydraulics plays a key role on biogeochemical processes and that the most important portion of the HZ is the zone with fast flows. The physical reasons for this dependence of production and reaction rates upon the local flux are unknown but we can speculate that it is related to the availability and delivery of resources (high velocities deliver resources more efficiently) and possibly due to the modification of and more efficient diffusion of nutrients through biofilms at high ambient velocities and turbulent flows (Hödl et al., 2014; Stewart, 2012). Our results also indicate that the processes within the oxic HZ with $\tilde{\tau}_{up}$ values from 0.5 to 1 because of their high velocities (flowpaths near the crest) may be the main sources of N_2O fluxes to the stream water, whereas anaerobic HZ ($\tilde{\tau}_{up}$ around 1.8) may produce the highest N_2O concentrations within the bulk of the HZ but may not contribute substantially to N_2O emissions to the stream, at least within the constraints of our experimental setup.

Funding Sources

This work was supported by NSF grant #1141690, #1141752, and # IIA-1301792.

Acknowledgments
We appreciate the cooperation of S. Nicol of Idaho State Parks with collecting sand. Bob Basham's help was critical in designing and implementing the flume experiments. Many others, including M. Lytle, C. Beeson, R. Hillsberry, L. Hoaks, M. Patterson, J. Fisher, and R. Will, provided assistance in setting up the experiment, collecting samples, and analyzing laboratory samples. All data used in this manuscript have been uploaded to Hydroshare (Reeder, Quick, Farrell, Benner, Feris, Marzadri, et al., 2018).

References

Anderson, B., Bartlett, K., Frolking, S., Hayhoe, K., Jenkins, J., & Salas, W. (2010). *Methane and nitrous oxide emissions from natural sources rep*. Washington, DC: EPA-430-R-10-001, EPA.

Beaulieu, J. J., Tank, J. L., Hamilton, S. K., Wollheim, W. M., Hall, R. O., Mulholland, P. J., et al. (2011). Nitrous oxide emission from denitrification in stream and river networks. *Proceedings of the National Academy of Sciences*, *108*(1), 214–219. https://doi.org/10.1073/pnas.1011464108

Beaulieu, J. J., Arango, C. P., Hamilton, S. K., & Tank, J. L. (2008). The production and emission of nitrous oxide from headwater streams in the Midwestern United States. *Global Change Biology*, *14*(4), 878–894. https://doi.org/10.1111/j.1365-2486.2007.01485.x

Benjankar, R., Tonina, D., Marzadri, A., McKean, J., & Isaak, D. J. (2016). Effects of habitat quality and ambient hyporheic flows on salmon spawning site selection. *Journal of Geophysical Research: Biogeosciences*, *121*(5), 1222–1235. https://doi.org/10.1002/2015JG003079

Budwig, R., & Goodwin, P. (2012). The Center for Ecohydraulics Research Mountain StreamLab - A facility for collaborative research and education. In *Innovations 2012: World innovations in engineering education and research* (pp. 17–29), edited. Maryland, USA: iNeer, Potomac.

Cardenas, M. B., & Wilson, J. L. (2007). Exchange across a sediment–water interface with ambient groundwater discharge. *Journal of Hydrology*, *346*(3–4), 69–80. https://doi.org/10.1016/j.jhydrol.2007.08.019

Chapelle, F. H. (1993). *Ground-water microbiology and geochemistry*. New York: John Wiley.

Davidson, E. A. (2009). The contribution of manure and fertilizer nitrogen to atmospheric nitrous oxide since 1860. *Nature Geoscience*, *2*(9), 659–662. http://www.nature.com/ngeo/journal/v2/n9/suppinfo/ngeo608_S1.html

Dietrich, J. T. (2017). Bathymetric structure-from-motion: Extracting shallow stream bathymetry from multi-view stereo photogrammetry. *Earth Surface Processes and Landforms*, *42*(2), 355–364. https://doi.org/10.1002/esp.4060

Elliott, A. H., & Brooks, N. H. (1997). Transfer of nonsorbing solutes to a streambed with bed forms: Theory. *Water Resources Research*, *33*(1), 123–136. https://doi.org/10.1029/96WR02784

Fehlman, H. M. (1985). *Resistance components and velocity distributions of open channel flows over bedforms* (p. 169). Fort Collins, CO.: Colorado State University.

Herzog, S. P., Higgins, C. P., & McCray, J. E. (2016). Engineered streambeds for induced hyporheic flow: Enhanced removal of nutrients, pathogens, and metals from urban streams. *Journal of Environmental Engineering*, *142*(1), 04015053. https://doi.org/10.1061/(ASCE)EE.1943-7870.0001012

Hilldale, R. C., & Raff, D. (2008). Assessing the ability of airborne LiDAR to map river bathymetry. *Earth Surface Processes and Landforms*, *33*(5), 773–783. https://doi.org/10.1002/esp.1575

Hödl, I., Mari, L., Bertuzzo, E., Suweis, S., Besemer, K., Rinaldo, A., & Battin, T. J. (2014). Biophysical controls on cluster dynamics and architectural differentiation of microbial biofilms in contrasting flow environments. *Environmental Microbiology*, *16*(3), 802–812. https://doi.org/10.1111/1462-2920.12205

Hudson, F. (2004). *Sample preparation and calculations for dissolved gas analysis in water samples using a GC headspace equilibration technique*, edited (pp. 1–14). Ada, OK: Ground Water and Ecosystems Restoration Division of the U.S. Environmental Protection Agency.

IPCC (2007). In Contribution of Working Group 1 to the Fourth Assessment Report of the Intergovernmental Panel on Climate Change Rep (Ed.), *Climate change 2007: The physical science basis* (p. 996). Cambridge, United Kingdom and New York, NY, USA: Intergovernmental Panel on Climate Change.

Javernick, L., Brasington, J., & Caruso, B. (2014). Modeling the topography of shallow braided rivers using structure-from-motion photogrammetry. *Geomorphology*, *213*, 166–182. https://doi.org/10.1016/j.geomorph.2014.01.006

Kinzel, P. J., Legleiter, C. J., & Nelson, J. M. (2013). Mapping river bathymetry with a small footprint green LiDAR: Applications and challenges[1]. *JAWRA Journal of the American Water Resources Association*, *49*(1), 183–204. https://doi.org/10.1111/jawr.12008

Laursen, A. E., & Seitzinger, S. P. (2004). Diurnal patterns of denitrification, oxygen consumption and nitrous oxide production in rivers measured at the whole-reach scale. *Freshwater Biology*, *49*(11), 1448–1458. https://doi.org/10.1111/j.1365-2427.2004.01280.x

Marzadri, A., Dee, M. M., Tonina, D., Bellin, A., & Tank, J. L. (2017). Role of surface and subsurface processes in scaling N_2O emissions along riverine networks. *Proceedings of the National Academy of Sciences*, *114*(17), 4330–4335. https://doi.org/10.1073/pnas.1617454114

Marzadri, A., Tonina, D., & Bellin, A. (2011). A semianalytical three-dimensional process-based model for hyporheic nitrogen dynamics in gravel bed rivers. *Water Resources Research*, *47*(11), W11518. https://doi.org/10.1029/2011WR010583

Marzadri, A., Tonina, D., & Bellin, A. (2013). Quantifying the importance of daily stream water temperature fluctuations on the hyporheic thermal regime: Implication for dissolved oxygen dynamics. *Journal of Hydrology*, *507*, 241–248. https://doi.org/10.1016/j.jhydrol.2013.10.030

Marzadri, A., Tonina, D., Bellin, A., & Tank, J. L. (2014). A hydrologic model demonstrates nitrous oxide emissions depend on streambed morphology. *Geophysical Research Letters*, *41*(15), 5484–5491. https://doi.org/10.1002/2014GL060732

Marzadri, A., Tonina, D., McKean, J. A., Tiedemann, M. G., & Benjankar, R. M. (2014). Multi-scale streambed topographic and discharge effects on hyporheic exchange at the stream network scale in confined streams. *Journal of Hydrology*, *519*, 1997–2011. https://doi.org/10.1016/j.jhydrol.2014.09.076

McMahon, P. B., & Dennehy, K. F. (1999). N2O emissions from a nitrogen-enriched river. *Environmental Science & Technology*, *33*(1), 21–25. https://doi.org/10.1021/es980645n

Ocampo, C. J., Oldham, C. E., & Sivapalan, M. (2006). Nitrate attenuation in agricultural catchments: Shifting balances between transport and reaction. *Water Resources Research*, *42*(1), W01408. https://doi.org/10.1029/2004WR003773

Otte, S., Grobben, N. G., Robertson, L. A., Jetten, M. S., & Kuenen, J. G. (1996). Nitrous oxide production by Alcaligenes faecalis under transient and dynamic aerobic and anaerobic conditions. *Applied and Environmental Microbiology*, *62*(7), 2421–2426.

Otte, S., Schalk, J., Kuenen, J. G., & Jetten, M. S. M. (1999). Hydroxylamine oxidation and subsequent nitrous oxide production by the heterotrophic ammonia oxidizer Alcaligenes faecalis. *Applied Microbiology and Biotechnology*, *51*(2), 255–261. https://doi.org/10.1007/s002530051390

Park, S., Croteau, P., Boering, K. A., Etheridge, D. M., Ferretti, D., Fraser, P. J., et al. (2012). Trends and seasonal cycles in the isotopic composition of nitrous oxide since 1940. *Nature Geoscience*, *5*(4), 261–265. http://www.nature.com/ngeo/journal/v5/n4/abs/ngeo1421.html#supplementary-information

Quick, A. M., Reeder, W. J., Farrell, T. B., Tonina, D., Feris, K. P., & Benner, S. G. (2016). Controls on nitrous oxide emissions from the hyporheic zones of streams. *Environmental Science & Technology*, *50*(21), 11,491–11,500. https://doi.org/10.1021/acs.est.6b02680

Ravishankara, A. R., Daniel, J. S., & Portmann, R. W. (2009). Nitrous oxide (N2O): The dominant ozone-depleting substance emitted in the 21st century. *Science*, *326*(5949), 123–125. https://doi.org/10.1126/science.1176985

Reeder, W. J., Quick, A. M., Farrell T. B., Benner S. G., Feris K. P., Marzadri A., & Tonina D. (2018), Spatially distributed, high-resolution nitrous oxide and residence time data for dune-like bedforms, edited, HydroShare. https://doi.org/10.4211/hs.8ed47eb4baee45eeaaa60f85b75b5042

Reeder, W. J., Quick, A. M., Farrell, T. B., Benner, S. G., Feris, K. P., & Tonina, D. (2018). Spatial and temporal dynamics of dissolved oxygen concentrations and bioactivity in the hyporheic zone. *Water Resources Research*, *54*(3), 2112–2128. https://doi.org/10.1002/2017WR021388

Rosamond, M. S., Thuss, S. J., & Schiff, S. L. (2012). Dependence of riverine nitrous oxide emissions on dissolved oxygen levels. *Nature Geoscience*, *5*(10), 715–718. http://www.nature.com/ngeo/journal/v5/n10/abs/ngeo1556.html#supplementary-information

Schreiber, F., Wunderlin, P., Udert, K. M., & Wells, G. F. (2012). Nitric oxide and nitrous oxide turnover in natural and engineered microbial communities: Biological pathways, chemical reactions, and novel technologies. *Frontiers in Microbiology*, *3*, 372. https://doi.org/10.3389/fmicb.2012.00372

Seitzinger, S. P., & Kroeze, C. (1998). Global distribution of nitrous oxide production and N inputs in freshwater and coastal marine ecosystems. *Global Biogeochemical Cycles*, *12*(1), 93–113. https://doi.org/10.1029/97GB03657

Stewart, P. S. (2012). Mini-review: Convection around biofilms. *Biofouling*, *28*(2), 187–198. https://doi.org/10.1080/08927014.2012.662641

Storlazzi, C. D., Dartnell, P., Hatcher, G. A., & Gibbs, A. E. (2016). End of the chain? Rugosity and fine-scale bathymetry from existing underwater digital imagery using structure-from-motion (SfM) technology. *Coral Reefs*, *35*(3), 889–894. https://doi.org/10.1007/s00338-016-1462-8

Tiedje, J. M. (1988). *Ecology of denitrification and dissimilatory nitrate reduction to ammonium*. New York: John Wiley.

Tonina, D., de Barros, F. P. J., Marzadri, A., & Bellin, A. (2016). Does streambed heterogeneity matter for hyporheic residence time distribution in sand-bedded streams? *Advances in Water Resources*, *96*, 120–126. https://doi.org/10.1016/j.advwatres.2016.07.009

Woodget, A. S., Carbonneau, P. E., Visser, F., & Maddock, I. P. (2015). Quantifying submerged fluvial topography using hyperspatial resolution UAS imagery and structure from motion photogrammetry. *Earth Surface Processes and Landforms*, *40*(1), 47–64. https://doi.org/10.1002/esp.3613

World Meteorological Organization (WMO) (2014), Scientific Assessment of Ozone Depletion: 2014, World Meteorological Organization, Global Ozone Research and Monitoring Project—Report No. 55Rep., 416 pp, Geneva, Switzerland.

Wuebbles, D. J. (2009). Nitrous oxide: No laughing matter. *Science*, *326*(5949), 56–57. https://doi.org/10.1126/science.1179571

Zarnetske, J. P., Haggerty, R., Wondzell, S. M., & Baker, M. A. (2011a). Dynamics of nitrate production and removal as a function of residence time in the hyporheic zone. *Journal of Geophysical Research*, *116*(G1), G01025. https://doi.org/10.1029/2010jg001356

Zarnetske, J. P., Haggerty, R., Wondzell, S. M., & Baker, M. A. (2011b). Labile dissolved organic carbon supply limits hyporheic denitrification. *Journal of Geophysical Research*, *116*(G4), G04036. https://doi.org/10.1029/2011JG001730

Zarnetske, J. P., Haggerty, R., Wondzell, S. M., Bokil, V. A., & González-Pinzón, R. (2012). Coupled transport and reaction kinetics control the nitrate source-sink function of hyporheic zones. *Water Resources Research*, *48*, W11508. https://doi.org/10.1029/2012WR011894